Multiple-Fano-resonance-induced fast and slow light in the hybrid nanomechanical-resonator system

Hua-Jun Chen*

School of Mechanics and Photoelectric Physics, Anhui University of Science and Technology, Huainan Anhui 232001, China

(Received 14 April 2021; revised 9 June 2021; accepted 28 June 2021; published 12 July 2021)

We investigate the multiple-Fano-resonance-induced fast and slow light in a hybrid nanomechanical-resonator (NR) system, where a doubly clamped suspended NR with an embedded quantum dot driven by two-tone fields is coupled to another two NRs with different frequencies via the Coulomb interaction. We display the absorption spectra of the weak probe field under different exciton-pump field detuning, and the sharp peaks in the absorption spectra are determined by the interaction between the NRs under the resonance. In the off-resonance, the absorption spectra can exhibit multiple Fano resonance, and the positions of the multiple Fano resonances are related to the interaction between the NRs and the frequencies of the different NRs. Furthermore, the multiple Fano resonances are accompanied by the rapid normal phase dispersion, which indicates the slow- and fast-light effect. We obtain that the group velocity index is tunable by the interaction between the NRs and the detuning, which can reach the conversion between the fast and slow light.

DOI: 10.1103/PhysRevA.104.013708

I. INTRODUCTION

Over the past decades, various techniques and progresses have been developed to reach fast and slow light in atomic vapors and solid-state devices, which need to control the group velocity index n_g of light pulses to make them propagate either $n_g < 0$ (fast light) or $n_g > 0$ (slow light) [1,2]. In order to realize the manipulation of light pulse propagation in different systems, kinds of techniques have been developed including electromagnetically induced transparency (EIT) [3–5], stimulated Brillouin scattering (SBS) [6,7], coherent population oscillation (CPO) [8], and Fano resonance [9–12]. In this work, we investigate the tunable and controllable fast and slow light in hybrid nanomechanical-resonator systems, which is mediated by different mechanical resonators.

Fano resonance presenting a asymmetric feature of a photoionization cross section in an atom was demonstrated by Fano [13], which is different from EIT in Λ-type atoms [5] leading to a symmetric transparency window. In EIT, an opaque medium can be made transparent due to quantum interference between two quantum pathways in Λ-type atoms, and the EIT technique has been applied extensively to control the group velocity of light [3,4], realized the storage of quantum information [14], obtained the enhanced nonlinear processes [15], and achieved optical switch [16] and quantum interference [17]. Compared with EIT, the Fano line profile shows an asymmetry shape caused by the scattering of light amplitude when the condition of observing EIT is not met and an extra frequency detuning is introduced. Since its discovery, Fano resonance has been a characteristic feature in different hybrid quantum systems, such as photonics crystal systems [18], graphene systems [19], plasmonic nanoparticles [11,20], quantum dots (QDs) [21,22], whispering-gallery modes [23–25], and electromagnetic metamaterials [26,27]. Moreover, many potential applications induced by Fano resonance have also been demonstrated in kinds of hybrid systems, which include sensors [28,29], enhanced light emission and transmission [30], electromagnetically induced absorption (EIA) [31], and the coherent optical propagation (such as slow light) [9,12]. In the coherent optical propagation, Fano resonances are characterized by a rapid steeper dispersion than conventional Lorentzian resonances, which promises the slow- or fast-light effect, and even tunable fast-to-slow light propagation (or vice versa).

On the other hand, nanomechanical resonators (NRs), due to their high natural frequencies and large quality factors [32], are applied to ultrasensitive detection of mechanical signal [33], mass [34,35], mechanical displacements [36], and spin [37]. Additionally, recent progress in nanotechnology has allowed the fabrication of hybrid systems including a single two-level system coupled to a NR [38–42], where the quantum nature of a macroscopic degree of freedom can be revealed and manipulated [43]. This opens up appealing perspectives for quantum information technologies [44], and for the exploration of the quantum-classical boundary. As a representative hybrid system, a two-level QD coupled to a NR has attracted much interest [45–47], which can be used to study fundamental quantum effects [48], and also it has possible applications in high precision measurement [49], zeptogram-scale mass sensing [50], and laser cooling of a NR mode to its quantum ground state [45].

In the present work, we propose a hybrid NR system, where a doubly clamped suspended NR with an embedded QD driven by two-tone fields couples to another two NRs with

*chenphysics@126.com

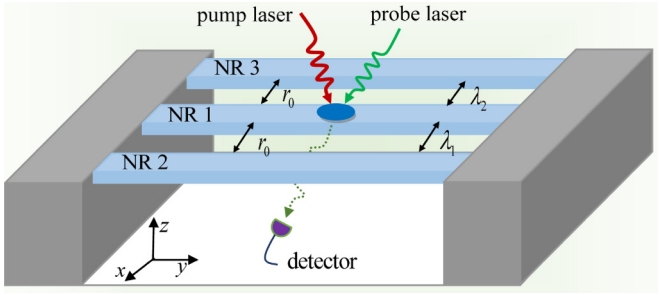

FIG. 1. Schematic diagram of the hybrid NRs system, where a doubly clamped suspended NR **1** with an embedded QD driven by two-tone fields is coupled to NR **2** and NR **3** via the Coulomb interaction with coupling strengths λ_1 and λ_2, respectively.

different frequencies via the Coulomb interaction. We first investigate the probe absorption spectra of the QD under the condition of resonance with controlling the coupling between the NRs, which presents a means to determine the frequencies of the NRs. Then, in the condition of detuning, the absorption and dispersion of the QD induced by the coupling between the NRs are also demonstrated, where the slope of the dispersion experiences the conversion from negative to positive and the absorption displays the asymmetric multiple Fano line shapes. The multiple Fano resonances can be effectively tuned and the probe absorption spectra can display a series of asymmetric Fano line shapes with tuning the detuning. Due to Fano resonances being characterized by a rapid steeper dispersion, the group velocity index n_g of light pulses can be accelerated and decreased significantly, which correspond to the negative and positive dispersion, respectively. Second, we investigate the slow light effect by numerically calculating the group delay of the probe field around the transparency window accompanied by the steep phase dispersion, and we find that a tunable and controllable fast-to-slow light propagation (and vice versa) can be achieved with manipulating the parametric regimes. However, the tunable slow and fast light phenomenon in our system is different from the previous NR system [51] which depends on the incident pump laser being on- and off-resonant with the exciton frequency; here, in our hybrid NRs system, we can obtain the conversion from fast to slow light with controlling the coupling between different NRs.

The paper is organized as follows. In Sec. II, we present the hybrid system and derive the analytical expression of the linear optical susceptibility and the group velocity index. In Sec. III, we discuss the absorption spectra under different parametric and detuning regimes, and especially in the off-resonance, the absorption spectra can exhibit multiple Fano resonance, which accompanies the rapid normal phase dispersion, which will lead to the slow- and fast-light effect. Finally, in Sec. IV, we conclude our results.

II. PHYSICAL PATTERN AND DYNAMICAL EQUATION

The system under consideration is sketched in Fig. 1, where a QD driven by a strong pump field and a weak probe field is embedded in NR **1** with frequency ω_{m1} coupled to NR **2** with frequencies ω_{m2} and NR **3** with frequency ω_{m3}, respectively, and the Hamiltonian of the hybrid system is given by [45,51–54]

$$\begin{aligned} H =& \hbar\omega_{ex}S^z + \hbar\omega_{m1}a_1^\dagger a_1 + \hbar\omega_{m2}a_2^\dagger a_2 + \hbar\omega_{m3}a_3^\dagger a_3 \\ &+ \hbar\omega_{m1}\beta S^z(a_1^\dagger + a_1) + \hbar\lambda_1(a_1^\dagger a_2 + a_1 a_2^\dagger) \\ &+ \hbar\lambda_2(a_1^\dagger a_3 + a_1 a_3^\dagger) - \mu\varepsilon_p(S^\dagger e^{-i\omega_p t} + S^- e^{i\omega_p t}) \\ &- \mu\varepsilon_s(S^\dagger e^{-i\omega_s t} + S^- e^{i\omega_s t}), \end{aligned} \tag{1}$$

where the first term indicates the Hamiltonian of the QD with the exciton frequency ω_{ex}. Here we consider that the QD is a two-level system including the ground state $|0\rangle$ and the single exciton state $|1\rangle$ [55,56] at low temperature. We introduce the pseudospin operators S^z and $S^\pm$ with the commutation relations $[S^z, S^\pm] = \pm S^\pm$ and $[S^+, S^-] = 2S^z$ to describe the QD. The second to fourth terms indicate the free Hamiltonian of the three NRs and we use creation (annihilation) operators $a_1^\dagger(a_1)$, $a_2^\dagger(a_2)$, and $a_3^\dagger(a_3)$ to describe the three NRs. The fifth term shows the coupling between NR **1** and QD with the coupling strength β, where the flexion induces extensions and compressions in the structure, and the longitudinal strain will modify the energy of the electronic states of QD through deformation potential coupling.

The sixth and seventh terms mean the interaction between NR **1** and NR **2** with coupling strength λ_1 and NR **1** and NR **3** with coupling strength λ_2, which can be realized via a substrate-mediated interaction [57] or the Coulomb interaction [54,58,59]. Here, we take the Coulomb interaction as an example, and we consider the interaction of NR **1** and NR **2** with frequencies ω_{m1} and ω_{m2}. The two resonators take the charges C_1V_1 and $-C_2V_2$, where $C_1(C_2)$ and $V_1(-V_2)$ being the capacitance and the voltage of the bias gate, respectively. Then the Coulomb coupling of the two resonators is $H_C = \frac{-C_1V_1C_2V_2}{4\pi\varepsilon_0|r_0+x_1-x_2|}$, where r_0 is the equilibrium distance between the two resonators, and x_1 and x_2 represent the small displacements of the two resonators from their equilibrium positions, respectively. Due to $r_0 \gg x_1, x_2$, with the second-order expansion, H_C can be rewritten as $H_C = \frac{-C_1V_1C_2V_2}{4\pi\varepsilon_0 r_0}[1 - \frac{x_1-x_2}{r_0} + (\frac{x_1-x_2}{r_0})^2]$, where the linear term may be absorbed into the definition of the equilibrium positions, and the quadratic term includes a renormalization of the oscillation frequency for the two resonators. Then we can obtain a reduced form $H_C = \hbar\lambda_1 x_1 x_2$ with $\lambda_1 = \frac{C_1V_1C_2V_2}{2\pi\hbar\varepsilon_0 r_0^3}$. Due to $x_1 = a_1^\dagger + a_1$ and $x_2 = a_2^\dagger + a_2$ being the position operators, then $H_C = \hbar\lambda_1(a_1^\dagger + a_1)(a_2^\dagger + a_2)$. When we neglected the nonconservation term of energy, we finally obtain $H_C = \hbar\lambda_1(a_1^\dagger a_2 + a_1 a_2^\dagger)$, i.e., the sixth term in Eq. (1). Using the same method, we can also obtain the seventh term of $\hbar\lambda_2(a_1^\dagger a_3 + a_1 a_3^\dagger)$.

The last two terms in Eq. (1) indicate the interactions between the QD and two laser fields including a strong pump field with frequency ω_p and a weak probe field with frequency ω_s simultaneously irradiating to the QD, where μ is the electric dipole moment of the exciton, ε_p and ε_s are the slowly varying envelope of the pump field and probe field, respectively. In a frame rotating with the frequency ω_p of the

pump field, Eq. (1) can be rewritten as

$$\begin{aligned} H =& \hbar\Delta_p S^z + \hbar\omega_{m1} a_1^\dagger a_1 + \hbar\omega_{m2} a_2^\dagger a_2 + \hbar\omega_{m3} a_3^\dagger a_3 \\ &+ \hbar\omega_{m1}\beta S^z (a_1^\dagger + a_1) + \hbar\lambda_1 (a_1^\dagger a_2 + a_1 a_2^\dagger) \\ &+ \hbar\lambda_2 (a_1^\dagger a_3 + a_1 a_3^\dagger) - \hbar\Omega_p (S^\dagger + S^-) \\ &- \mu\varepsilon_s (S^\dagger e^{-i\delta t} + S^- e^{i\delta t}), \end{aligned} \tag{2}$$

where $\Delta_p = \omega_{ex} - \omega_p$ is the exciton-pump field detuning, $\delta = \omega_s - \omega_p$ is the probe-pump detuning, and $\Omega_p = \mu\varepsilon_p/\hbar$ is the Rabi frequency of the pump field. The Heisenberg-Langevin equations of the operators including the corresponding noise and damping terms can be written as follows [60]:

$$\partial_t S^z = -\Gamma_1 (S^z + 1/2) + i\Omega_p (S^+ - S^-) + \frac{i\mu\varepsilon_s}{\hbar} (S^+ e^{-i\delta t} - S^- e^{i\delta t}), \tag{3}$$

$$\partial_t S^- = -(i\Delta_p + \Gamma_2) S^- - i\omega_{m1}\beta x_1 S^- - 2i\Omega_p S^z - \frac{2i\mu\varepsilon_s S^z e^{-i\delta t}}{\hbar} + \tau_{in}, \tag{4}$$

$$\partial_t^2 x_1 + \gamma_{m1}\partial_t x_1 + \omega_{m1}'^2 x_1 + \lambda_1' x_2 + \lambda_2' x_3 = -2\omega_{m1}^2 \beta S^z + \xi_1, \tag{5}$$

$$\partial_t^2 x_2 + \gamma_{m2}\partial_t x_2 + \omega_{m2}'^2 x_2 + \lambda_1' x_1 + \lambda_{12} x_3 = -2\lambda_1\omega_{m1}\beta S^z + \xi_2, \tag{6}$$

$$\partial_t^2 x_3 + \gamma_{m3}\partial_t x_3 + \omega_{m3}'^2 x_3 + \lambda_2' x_1 + \lambda_{12} x_2 = -2\lambda_2\omega_{m1}\beta S^z + \xi_3, \tag{7}$$

where Γ_1 (Γ_2) is the exciton relaxation rate (exciton dephasing rate), and γ_{m1}, γ_{m2}, and γ_{m3} are the decay rate of the three NRs. $\omega_{m1}'^2 = \omega_{m1}^2 + \lambda_1^2 + \lambda_2^2$, $\omega_{m2}'^2 = \omega_{m2}^2 + \lambda_1^2$, $\omega_{m3}'^2 = \omega_{m3}^2 + \lambda_2^2$, $\lambda_1' = \lambda_1(\omega_{m1} + \omega_{m2})$, $\lambda_2' = \lambda_2(\omega_{m1} + \omega_{m3})$, and $\lambda_{12} = \lambda_1\lambda_2$. τ_{in} is the δ-correlated Langevin noise operator with zero mean, and ξ_k is Langevin force arising from the interaction between the kth mechanical resonator and its environment.

Using $\rho = \rho_0 + \delta\rho$ (ρ indicates the operators: S^z, S^-, x_1, x_2, x_3), Eqs. (3)– (7) can be divided into the steady parts and the fluctuation ones. Substituting the division forms into Eqs. (3)– (7) and setting all the time derivations at the steady parts to be zero, we obtain the steady state solutions of the variables as follows:

$$\Gamma_1(w_0 + 1) = 2i\Omega_p(S_0^* - S_0), \tag{8}$$

$$(i\Delta_p + \Gamma_2) S_0 + i\omega_{m1}\beta x_{10} S_0 = -iw_0\Omega_p, \tag{9}$$

$$\omega_{m1}'^2 x_{10} + \lambda_1' x_{20} + \lambda_2' x_{30} = -w_0\omega_{m1}^2\beta, \tag{10}$$

$$\omega_{m2}'^2 x_{20} + \lambda_1' x_{10} + \lambda_{12} x_{30} = -w_0\omega_{m1}\beta\lambda_1, \tag{11}$$

$$\omega_{m3}'^2 x_{30} + \lambda_2' x_{10} + \lambda_{12} x_{20} = -w_0\omega_{m1}\beta\lambda_2, \tag{12}$$

which determine the steady-state population inversion ($w_0 = 2S_0^z$) of the exciton. As all the pump fields are assumed to be sufficiently strong, all the operators can be identified with their expectation values under the mean-field approximation $\langle Qc\rangle = \langle Q\rangle\langle c\rangle$ [61]. After being linearized by neglecting nonlinear terms in the fluctuations, the Langevin equations for the expectation values are

$$\langle\partial_t \delta S^z\rangle = -\Gamma_1\langle\delta S^z\rangle + i\Omega_p(\langle\delta S^+\rangle - \langle\delta S^-\rangle) + \frac{i\mu\varepsilon_s}{\hbar}[S_0^* e^{-i\delta t} - S_0 e^{i\delta t}], \tag{13}$$

$$\langle\partial_t \delta S^-\rangle = -(i\Delta_p' + \Gamma_2)\langle\delta S^-\rangle - i\omega_{m1}\beta S_0\langle\delta x_1\rangle - 2i\Omega_p\langle\delta S^z\rangle - \frac{i\mu w_0\varepsilon_s}{\hbar} e^{-i\delta t}, \tag{14}$$

$$\left\langle\partial_t^2\delta x_1\right\rangle + \gamma_{m1}\langle\partial_t\delta x_1\rangle + \omega_{m1}'^2\langle\delta x_1\rangle + \lambda_1'\langle\delta x_2\rangle + \lambda_2'\langle\delta x_3\rangle = -2\omega_{m1}^2\beta\langle\delta S^z\rangle, \tag{15}$$

$$\left\langle\partial_t^2\delta x_2\right\rangle + \gamma_{m2}\langle\partial_t\delta x_2\rangle + \omega_{m2}'^2\langle\delta x_2\rangle + \lambda_1'\langle\delta x_1\rangle + \lambda_{12}\langle\delta x_3\rangle = -2\lambda_1\omega_{m1}\beta\langle\delta S^z\rangle, \tag{16}$$

$$\left\langle\partial_t^2\delta x_3\right\rangle + \gamma_{m3}\langle\partial_t\delta x_3\rangle + \omega_{m3}'^2\langle\delta x_3\rangle + \lambda_2'\langle\delta x_1\rangle + \lambda_{12}\langle\delta x_2\rangle = -2\lambda_2\omega_{m1}\beta\langle\delta S^z\rangle, \tag{17}$$

which is a set of nonlinear equations and the steady-state response in the frequency domain is composed of many frequency components. $\Delta_p' = \Delta_p + \omega_{m1}\beta w_0\alpha$, where

$$\alpha = \frac{\beta\omega_{m1}^2\left(\omega_{m2}'^2\omega_{m3}'^2 - \lambda_{12}^2\right) + \lambda_1\omega_{m1}\beta\left(\lambda_2'\lambda_{12} - \lambda_1'\omega_{m3}'^2\right) + \lambda_2\omega_{m1}\beta\left(\lambda_1'\lambda_{12} - \lambda_2'\omega_{m2}'^2\right)}{\omega_{m3}'^2\lambda_1'^2 - 2\lambda_1'\lambda_2'\lambda_{12} + \omega_{m2}'^2\lambda_2'^2 + \omega_{m1}'^2\lambda_{12}^2 - \omega_{m1}'^2\omega_{m2}'^2\omega_{m3}'^2}. \tag{18}$$

To solve these equations, we make the ansatz [62] $\langle\delta\rho\rangle = \rho_+ e^{-i\delta t} + \rho_- e^{i\delta t}$, and substituting it into Eqs. (13)–(17), ignoring the second-order terms, and working to the lowest order in ε_s but to all orders in ε_p, we obtain the linear optical susceptibility as

$\chi^{(1)}_{\rm eff}(\omega_s) = \mu S_+(\omega_s)/\varepsilon_s = (\mu^2/\hbar\Gamma_2)\chi^{(1)}(\omega_s)$, and $\chi^{(1)}(\omega_s)$ is given by

$$\chi^{(1)}(\omega_s) = \frac{[\Sigma_4\theta_2 - \theta_1\theta_8]\Gamma_2}{\Sigma_1\Sigma_4 + \theta_1\theta_7}, \tag{19}$$

where

$$\Pi_1 = \frac{\lambda_1'}{\omega_{m1}'^2 - i\gamma_{m1}\delta - \delta^2}, \quad \Pi_2 = \frac{\lambda_2'}{\omega_{m1}'^2 - i\gamma_{m1}\delta - \delta^2}, \quad \eta_1 = \frac{-2\omega_{m1}^2\beta}{\omega_{m1}'^2 - i\gamma_{m1}\delta - \delta^2},$$

$$\Pi_3 = \frac{\lambda_1'}{\omega_{m2}'^2 - i\gamma_{m2}\delta - \delta^2}, \quad \Pi_4 = \frac{\lambda_{12}}{\omega_{m2}'^2 - i\gamma_{m2}\delta - \delta^2}, \quad \eta_2 = \frac{-2\lambda_1\omega_{m1}\beta}{\omega_{m2}'^2 - i\gamma_{m2}\delta - \delta^2},$$

$$\Pi_5 = \frac{\lambda_2'}{\omega_{m3}'^2 - i\gamma_{m3}\delta - \delta^2}, \quad \Pi_6 = \frac{\lambda_{12}}{\omega_{m3}'^2 - i\gamma_{m3}\delta - \delta^2}, \quad \eta_3 = \frac{-2\lambda_2\omega_{m1}\beta}{\omega_{m3}'^2 - i\gamma_{m3}\delta - \delta^2},$$

$$\Lambda = \frac{(\Pi_4\Pi_6 - 1)\eta_1 + (\Pi_1 - \Pi_2\Pi_6)\eta_2 + (\Pi_2 - \Pi_1\Pi_4)\eta_3}{(\Pi_4\Pi_6 - 1) + \Pi_5(\Pi_2 - \Pi_1\Pi_4) + \Pi_3(\Pi_1 - \Pi_2\Pi_6)}, \quad \theta_1 = \frac{2\Omega_p^2 + \omega_{m1}\beta S_0\Lambda\Omega_p}{\Gamma_1 - i\delta},$$

$$\theta_2 = \frac{S_0^*(\omega_{m1}\beta S_0\Lambda + 2\Omega_p) - iw_0(\Gamma_1 - i\delta)}{\Gamma_1 - i\delta}, \quad \theta_3 = \frac{2\Omega_p^2 + \omega_{m1}\beta S_0\Lambda^*\Omega_p}{\Gamma_1 + i\delta},$$

$$\theta_4 = \frac{\mu\varepsilon_s S_0(\omega_{m1}\beta S_0\Lambda^* + 2\Omega_p)}{\Gamma_1 + i\delta}, \quad \theta_5 = -\frac{2\Omega_p^2 + \omega_{m1}\beta S_0^*\Lambda^*\Omega_p}{\Gamma_1 + i\delta},$$

$$\theta_6 = \frac{\mu\varepsilon_s S_0(\omega_{m1}\beta S_0^*\Lambda^* + 2\Omega_p) - i\mu\varepsilon_s w_0(\Gamma_1 + i\delta)}{\Gamma_1 + i\delta}, \quad \theta_7 = -\frac{2\Omega_p^2 + \omega_{m1}\beta S_0^*\Lambda\Omega_p}{\Gamma_1 - i\delta},$$

$$\theta_8 = \frac{\mu\varepsilon_s S_0^*(\omega_{m1}\beta S_0^*\Lambda + 2\Omega_p)}{\Gamma_1 - i\delta}, \quad \Sigma_1 = i\Delta_p' + \Gamma_2 - i\delta + \theta_1, \quad \Sigma_2 = i\Delta_p' + \Gamma_2 + i\delta + \theta_3,$$

$$\Sigma_3 = -i\Delta_p' + \Gamma_2 + i\delta - \theta_5, \quad \Sigma_4 = -i\Delta_p' + \Gamma_2 - i\delta - \theta_7, \tag{20}$$

The imaginary and real parts of $\chi^{(1)}(\omega_s)$ indicate absorption and dispersion, respectively.

As the light group velocity is [63,64] $\upsilon_g = c/[n + \omega_s(dn/d\omega_s)]$, where $n \approx 1 + 2\pi\chi^{(1)}_{\rm eff}$, then we obtain

$$c/\upsilon_g = 1 + 2\pi{\rm Re}\chi^{(1)}_{\rm eff}(\omega_s)_{\omega_s=\omega_{ex}} + 2\pi\omega_s{\rm Re}\left(d\chi^{(1)}_{\rm eff}/d\omega_s\right)_{\omega_s=\omega_{ex}}. \tag{21}$$

Obviously, when ${\rm Re}\chi^{(1)}_{\rm eff}(\omega_s)_{\omega_s=\omega_{ex}} = 0$, the dispersion is steeply positive or negative, and the group velocity is significantly reduced or increased. We further define the group velocity index n_g as

$$n_g = \frac{c}{\upsilon_g} - 1 = \frac{c - \upsilon_g}{\upsilon_g} = \frac{2\pi\omega_{ex}\rho\mu^2}{\hbar\Gamma_2}{\rm Re}\left(\frac{d\chi^{(1)}_{\rm eff}}{d\omega_s}\right)_{\omega_s=\omega_{ex}} = \Gamma_2\Sigma{\rm Re}\left(\frac{d\chi^{(1)}_{\rm eff}}{d\omega_s}\right)_{\omega_s=\omega_{ex}}, \tag{22}$$

where $\Sigma = 2\pi\omega_{ex}\rho\mu^2/\hbar\Gamma_2^2$. One can observe the slow light if $n_g > 0$, and the superluminal light when $n_g < 0$ [2].

We use the realistic hybrid QD-NR system to illustrate the numerical results [45]: the exciton relaxation rate $\Gamma_1 =$ 0.3 GHz, and the exciton dephasing rate $\Gamma_2 = 0.15$ GHz. The physical parameters of GaAs NR **1** are $(\omega_{m1}, m, Q) =$ (1.2 GHz, 5.3×10^{-15} g, 3×10^4), where m and Q are the effective mass and quality factor of the NR **1**, respectively. The decay rate of the NR **1** is $\gamma_m = \omega_m/Q = 4 \times 10^{-5}$ GHz, the coupling strength between QD and NR **1** is $\beta = 0.06$, and the frequencies of another two NRs are $\omega_{m2} = 0.9\omega_{m1}$, $\omega_{m3} = 1.1\omega_{m1}$.

III. NUMERICAL RESULTS AND DISCUSSION

We first show the probe absorption, i.e., the imaginary part (${\rm Im}\chi^{(1)}$) of linear optical susceptibility, as a function of probe-exciton detuning $\Delta_s = \omega_s - \omega_{ex}$ on the condition of resonance (i.e., $\Delta_p = 0$) under different parameter regimes as shown in Fig. 2. In Fig. 2(a), the interaction of NR **1** and NR **2** is $\lambda_1 = 0$ and NR **1** and NR **3** is $\lambda_2 = 0$, i.e., only NR **1** in the system and two sharp sideband peaks at both sides of the probe absorption spectrum just correspond to the frequency of the NR **1** with frequency $\omega_{m1} = 1.2$ GHz. The physical origin of the phenomenon has been demonstrated in a coupled NR system [35]. In Fig. 2(b), we consider the case of $\lambda_1 = 0.1\omega_{m1}$ and $\lambda_2 = 0$ with the resonator frequencies $\omega_{m1} = 1.2$ GHz, $\omega_{m2} = 0.9\omega_{m1}$, and $\omega_{m3} = 1.1\omega_{m1}$. We find that four sharp sideband peaks appear in the probe absorption spectrum, and the peaks locate at $\pm\omega_{m1} \pm \lambda_1$ and $\pm\omega_{m2} \mp \lambda_1$, i.e., $\pm 1.1\omega_{m1}$ and $\pm 0.8\omega_{m1}$, respectively. In Fig. 2(c), the parameter regimes are $(\lambda_1 = 0, \lambda_2 = 0.1\omega_{m1})$ and $(\omega_{m1} =$ 1.2 GHz, $\omega_{m2} = 0.9\omega_{m1}$, $\omega_{m3} = 1.1\omega_{m1})$; four sharp sideband peaks locating at $\pm\omega_{m3} \pm \lambda_2$ and $\pm\omega_{m1} \mp \lambda_2$, i.e., $\pm 1.2\omega_{m1}$ and $\pm 0.9\omega_{m1}$, respectively, appear in the probe absorption spectrum. In Fig. 2(d), both NR **2** and NR **3** are also considered that couple to NR **1**, i.e., $\lambda_1 = 0.1\omega_{m1}$ and $\lambda_2 = 0.1\omega_{m1}$, and we consider the frequencies of the three NRs:

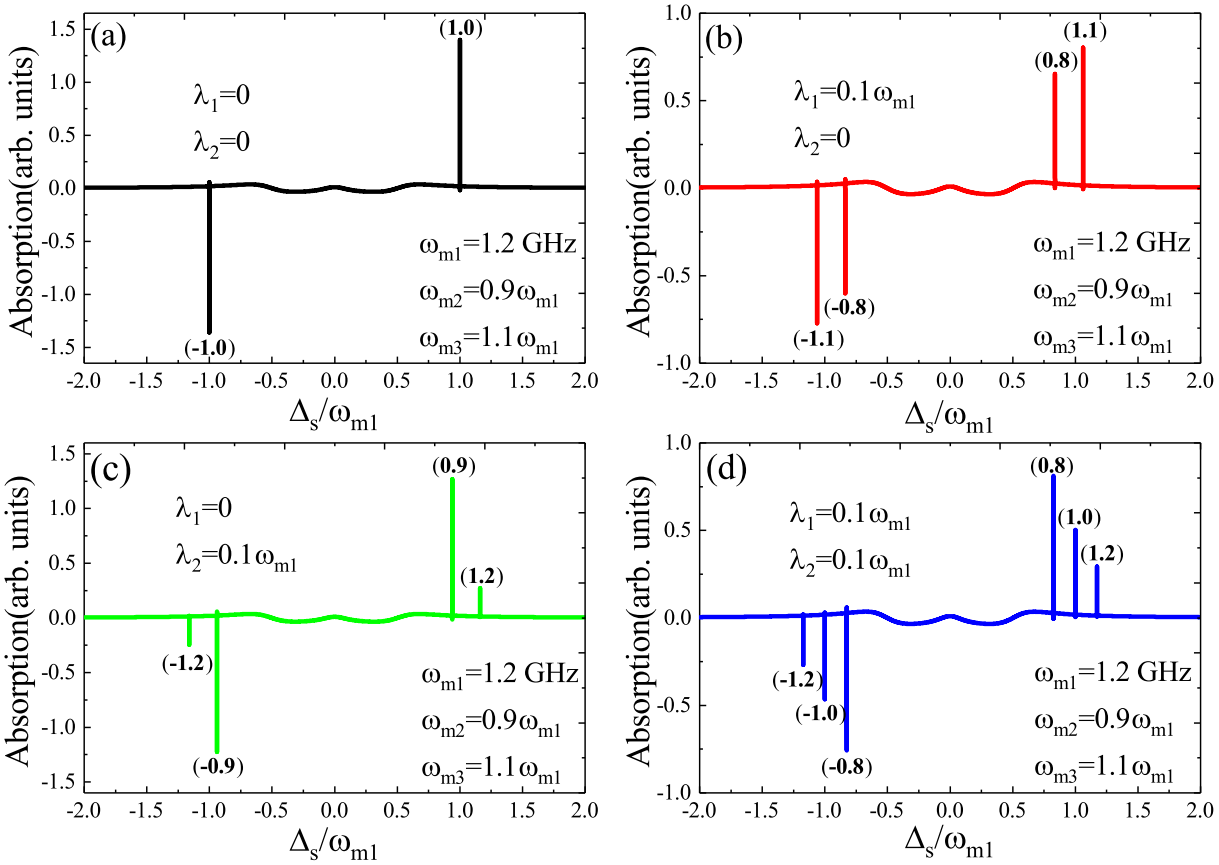

FIG. 2. The probe absorption spectra as a function of probe-exciton detuning $\Delta_s = \omega_s - \omega_{ex}$ on the condition of resonance ($\Delta_p = 0$) for different parameter regimes. (a) $\lambda_1 = 0$, $\lambda_2 = 0$; (b) $\lambda_1 = 0.1\omega_{m1}$, $\lambda_2 = 0$; (c) $\lambda_1 = 0$, $\lambda_2 = 0.1\omega_{m1}$; (d) $\lambda_1 = 0.1\omega_{m1}$, $\lambda_2 = 0.1\omega_{m1}$. The other parameters are $\omega_{m1} = 1.2$ GHz, $\omega_{m2} = 0.9\omega_{m1}$, $\omega_{m3} = 1.1\omega_{m1}$, and $\Omega_p^2 = 0.1$ (GHz)^2.

$\omega_{m1} = 1.2$ GHz, $\omega_{m2} = 0.9\omega_{m1}$, $\omega_{m3} = 1.1\omega_{m1}$. It is obvious that six sharp sideband peaks appear in the probe absorption spectrum, which locate at $\pm\omega_{m3} \pm \lambda_2$, $\pm\omega_{m1}$, and $\pm\omega_{m2} \mp \lambda_1$, i.e., $\pm 1.2\omega_{m1}$, $\pm\omega_{m1}$, and $\pm 0.8\omega_{m1}$, respectively. Therefore, the locations of the sharp peaks in the absorption spectrum are determined by the coupling strengths between the three NRs and their resonator frequencies, and we can also present a means to measure the frequencies of the NRs.

Second, switching the detuning Δ_p from the resonance ($\Delta_p = 0$) to the red sideband ($\Delta_p = \omega_{m1}$), we investigate the evolution of the absorption ($\mathrm{Im}\chi^{(1)}$) for different coupling strengths with different frequencies of NRs (such as $\omega_{m1} = 1.2$ GHz, $\omega_{m2} = 0.9\omega_{m1}$, and $\omega_{m3} = 1.1\omega_{m1}$) as shown in Figs. 3(a1)–3(a4), and Figs. 3(b1)–3(b4) are the details corresponding to Figs. 3(a1)–3(a4), respectively. In Fig. 3(a1), the coupling strengths between the three NRs are $\lambda_1 = 0$ and $\lambda_2 = 0$, i.e., only in NR **1** in our hybrid system does the imaginary part exhibit zero absorption at $\Delta_s = 0$ as shown the detail in Fig. 3(b1), i.e., transparent transmission without any absorption, which was termed as phonon-induced transparency [65] due to mechanically induced coherent population oscillation when the pump-probe detuning $\delta = \omega_s - \omega_p$ equals the resonator frequency ω_{m1} [35]. As demonstrated in cavity optomechanical systems, the appearance of a transparent window around $\Delta_s = 0$ in the probe transmission spectrum (here, in our hybrid system, it is the probe absorption spectrum) will lead to the slow light effect [61,66–68]. In Figs. 3(a2) and 3(a3), the coupling strengths between the three NRs are ($\lambda_1 = 0.1\omega_{m1}$, $\lambda_2 = 0$) and ($\lambda_1 = 0$, $\lambda_2 = 0.1\omega_{m1}$), i.e., there are two NRs (NR **1** and NR **2**, or NR **1** and NR **3**) in the system. We find that not only the zero absorption peak around $\Delta_s \approx 0$ but also a Fano resonance peak induced by another NR appear in the absorption spectrum. The location of the sharp peaks are related to the coupling strengths of NRs and the resonator frequencies as shown the detail in Figs. 3(b2) and 3(b3). If the system includes three NRs (i.e., NR **1**, NR **2**, and NR **3**), it is obvious that three absorption peaks appear in the probe absorption spectrum, which includes one peak around $\Delta_s = 0$ like in Fig. 3(a4) and another two Fano peaks induced by another two different NRs (NR **2** with frequency $\omega_{m2} = 0.9\omega_{m1}$ and NR **3** with frequency $\omega_{m2} = 1.1\omega_{m1}$) under the coupling strengths of the three NRs $\lambda_1 = 0.1\omega_{m1}$ and $\lambda_2 = 0.1\omega_{m1}$ as shown in the detail in Fig. 3(b4).

As to the dispersion (i.e., the real part of the linear optical susceptibility $\mathrm{Re}\chi^{(1)}$), we also plot the evolution of the dispersion $\mathrm{Re}\chi^{(1)}$ as a function of Δ_s under the red sideband ($\Delta_p = \omega_{m1}$) for different coupling strengths with the NR frequencies $\omega_{m1} = 1.2$ GHz, $\omega_{m2} = 0.9\omega_{m1}$, and $\omega_{m3} = 1.1\omega_{m1}$ as shown in Figs. 3(c1)–3(c4), and Figs. 3(d1)–3(d4) are the details corresponding to Figs. 3(c1)–3(c4), respectively. Figures 3(c1) and 3(c4) give the dispersion under the coupling regimes: ($\lambda_1 = 0$, $\lambda_2 = 0$) and ($\lambda_1 = 0.1\omega_{m1}$, $\lambda_2 = 0.1\omega_{m1}$), respectively; it is obvious that the dispersion, exhibiting the positive steep slope at $\Delta_s = 0$, which combines the zero

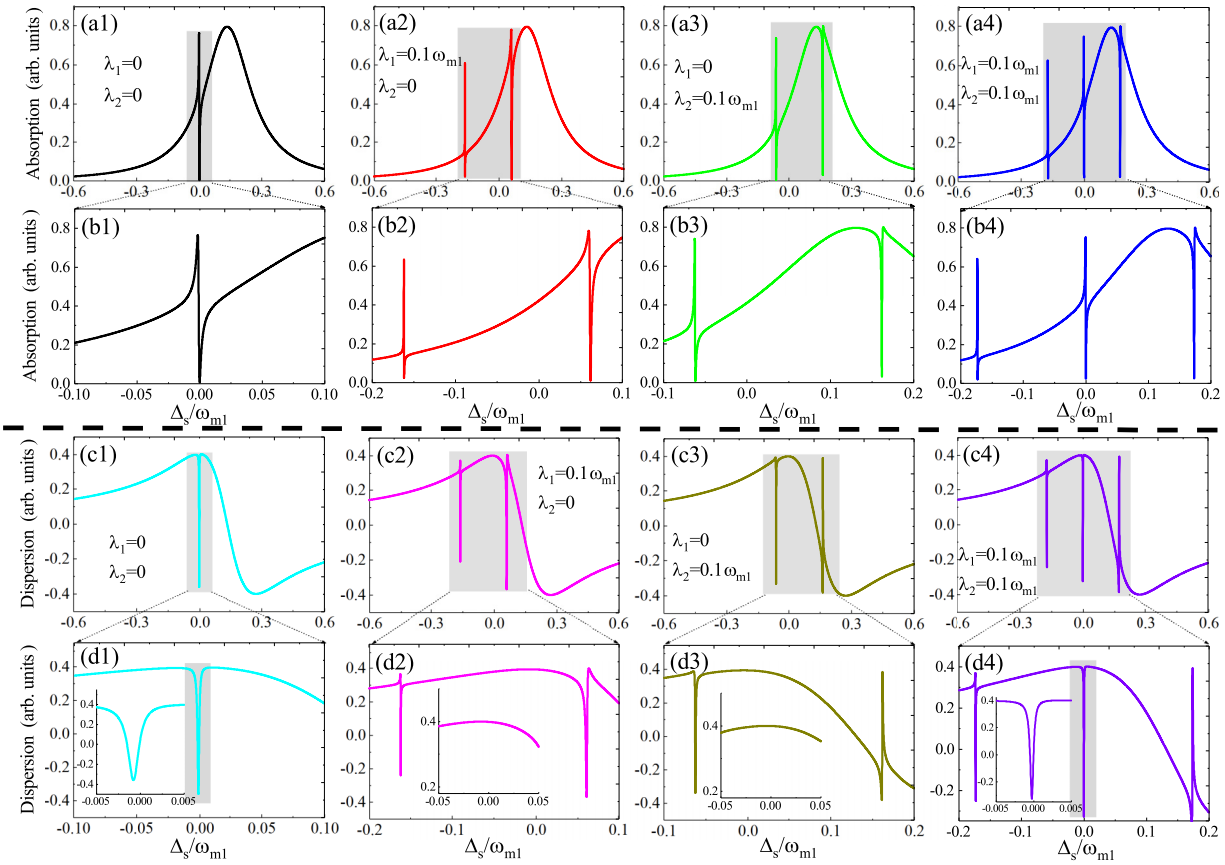

FIG. 3. The absorption as a function of Δ_s at the red sideband $\Delta_p = \omega_{m1}$ for different coupling regimes: (a1) $\lambda_1 = 0$ and $\lambda_2 = 0$; (a2) $\lambda_1 = 0.1\omega_{m1}$ and $\lambda_2 = 0$; (a3) $\lambda_1 = 0$ and $\lambda_2 = 0.1\omega_{m1}$; (a4) $\lambda_1 = 0.1\omega_{m1}$ and $\lambda_2 = 0.1\omega_{m1}$. Panels (b1)–(b4) are the details corresponding to (a1)–(a4). The dispersion as a function of Δ_s at the red sideband $\Delta_p = \omega_{m1}$ for different coupling regimes: (c1) $\lambda_1 = 0$ and $\lambda_2 = 0$; (c2) $\lambda_1 = 0.1\omega_{m1}$ and $\lambda_2 = 0$; (c3) $\lambda_1 = 0$ and $\lambda_2 = 0.1\omega_{m1}$; (c4) $\lambda_1 = 0.1\omega_{m1}$ and $\lambda_2 = 0.1\omega_{m1}$. Panels (d1)–(d4) are the details corresponding to (c1)–(c4). The insets in (d1)–(d4) are the amplification of (d1)–(d4) around $\Delta_s = 0$. The other parameters are $\omega_{m1} = 1.2$ GHz, $\omega_{m2} = 0.9\omega_{m1}$, $\omega_{m3} = 1.1\omega_{m1}$, and $\Omega_p^2 = 0.1$ (GHz)^2.

absorption at $\Delta_s = 0$ in Figs. 3(a1) and 3(a4), will lead to the slow light effect. In Figs. 3(d1) and 3(d4), we give the details of Figs. 3(c1) and (c4), and the difference of Figs. 3(c1) and 3(c4) is that the dispersion in Fig. 3(c4) shows three peaks at the conditions of $\lambda_1 = 0.1\omega_{m1}$ and $\lambda_2 = 0.1\omega_{m1}$. When we further magnify the dispersion around $\Delta_s = 0$ as shown the insets in Figs. 3(d1) and 3(d4), obviously the positive steep slope is steeper in the coupling regimes ($\lambda_1 = 0.1\omega_{m1}$, $\lambda_2 = 0.1\omega_{m1}$) than in ($\lambda_1 = 0$, $\lambda_2 = 0$). In other words, if the hybrid system includes three NRs (i.e., NR **1**, NR **2**, and NR **3**), the slow light effect will be more remarkable in the single NR system (i.e., only NR **1**). In Figs. 3(c2) and 3(c3), we display the dispersion under the coupling regimes of ($\lambda_1 = 0.1\omega_{m1}$, $\lambda_2 = 0$) and ($\lambda_1 = 0$, $\lambda_2 = 0.1\omega_{m1}$), which correspond to the system including two NRs i.e., NR **1** and NR **2,** or NR **1** and NR **3**, and Figs. 3(d2) and 3(d3) are their details. We can see that the dispersion shows the negative steep slope around $\Delta_s = 0$ as shown in the insets in Figs. 3(d2) and 3(d3), which will result in the fast light effect.

No matter what regimes induce the zero absorption, once a transparency window appears in the probe absorption spectra, the remarkable phenomena of slow light or fast light can appear in the hybrid system. When the transparency appears in the absorption, the slope around the transparency window of the dispersion will experience the conversion between the negative to positive. As we know, the positive steep slope of dispersion will induce the group velocity index $n_g > 0$, then the slow light phenomenon will appear in the system. Conversely, if the dispersion shows the negative steep slope, the group velocity index $n_g < 0$, and the fast light will be achieved. Figure 4 plots the group velocity index n_g versus the Rabi frequency Ω_p^2 for the NR frequencies $\omega_{m1} = 1.2$ GHz, $\omega_{m2} = 0.9\omega_{m1}$, $\omega_{m3} = 1.1\omega_{m1}$ at the red sideband $\Delta_p = \omega_{m1}$. When one NR with coupling regimes ($\lambda_1 = 0$, $\lambda_2 = 0$) corresponding to Figs. 3(a1) and 3(c1) or three NRs with coupling regimes ($\lambda_1 = 0.1\omega_{m1}$, $\lambda_2 = 0.1\omega_{m1}$) corresponding to Figs. 3(a4) and 3(c4) are in the system, one can see that the group velocity index n_g is positive varying with the Rabi frequency Ω_p^2, which represents the slow light effect, and the slow light effect in three NRs (the dot dash red line) is more significant than in the single NR (the black solid line) system. However, when two NRs are considered, i.e., NR **1** and NR **2** with coupling regimes ($\lambda_1 = 0.1\omega_{m1}$, $\lambda_2 = 0$) corresponding to Figs. 3(a2) and 3(c2) or NR **1** and NR **3** with coupling regimes ($\lambda_1 = 0$, $\lambda_2 = 0.1\omega_{m1}$) corresponding to Figs. 3(a3) and 3(c3) in the hybrid system, we find that the group velocity index n_g manifests the fast light effect as shown the inset in Fig. 4. Although the fast light effect was demonstrated in a

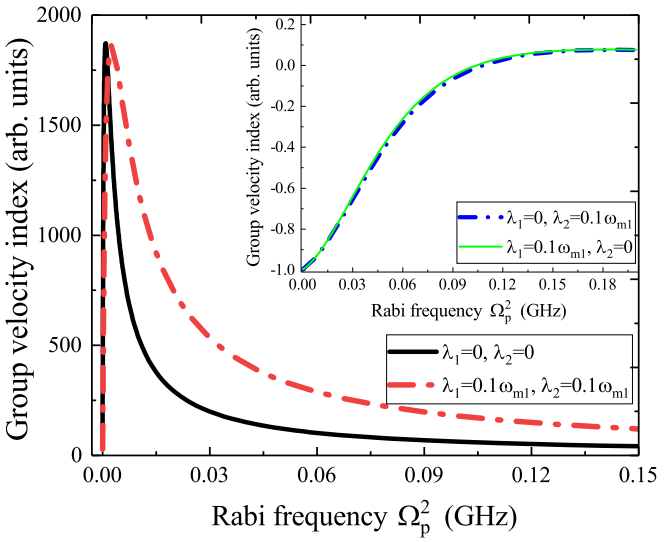

FIG. 4. The group velocity index n_g vs Rabi frequency Ω_p^2 for four different coupling strengths of λ_1 and λ_2 in the parameters of $\omega_{m1} = 1.2$ GHz, $\omega_{m2} = 0.9\omega_{m1}$, $\omega_{m3} = 1.1\omega_{m1}$ under the red sideband $\Delta_p = \omega_{m1}$.

carbon nanotube resonator [51], which needs the condition of resonance ($\Delta_p = 0$), in our hybrid system, the fast light effect can even be achieved at the red sideband $\Delta_p = \omega_{m1}$ by controlling the coupling strengths between the three NRs.

In Fig. 5, we further present the absorption and dispersion profiles as a function of the probe detuning Δ_s at the fixed coupling strengths ($\lambda_1 = 0.1\omega_{m1}$, $\lambda_2 = 0.1\omega_{m1}$) and the frequency of the NRs ($\omega_{m1} = 1.2$ GHz, $\omega_{m2} = 0.9\omega_{m1}$, $\omega_{m3} = 1.1\omega_{m1}$) for different pump detuning Δ_p. The left parts show the absorption, and it is obvious that the triple-Fano resonances appear in the absorption spectra, where the middle Fano resonance is induced by the coupling between exciton and NR **1** causing quantum interference between NR **1** and the two optical fields via the exciton as $\delta = \omega_{m1}$, and the right and the left Fano resonance come from the NR **1** coupling to the NR **2** and NR **3**. In addition, with increasing the detuning Δ_p from $\Delta_p = 0.7\omega_{m1}$ to $\Delta_p = 1.3\omega_{m1}$, the middle Fano resonance moves to the right. The right parts plot the dispersion, and we show that the evolutionary process of the dispersion as a function of Δ_s with increasing detuning Δ_p from $\Delta_p = 0.7\omega_{m1}$ to $\Delta_p = 1.3\omega_{m1}$, which combines the absorption, will induce the slow light effect because the dispersion manifests a positive steep slope around $\Delta_s = 0$. The details of absorption and dispersion around $\Delta_s = 0$ are presented in the following figures.

Then, in Fig. 6(a), we give the details of the absorption in Fig. 5 around $\Delta_s = 0$; the absorption spectra present asymmetrical zero absorption deep (i.e., Fano resonance) and the Fano shapes are changed significantly under different detuning Δ_p. In Fig. 6(b), the details of the dispersion in Fig. 5 around $\Delta_s = 0$ are also plotted, and the dispersion experiences the conversion from peak to deep with increasing the detuning Δ_p from $\Delta_p = 0.7\omega_{m1}$ to $\Delta_p = 1.3\omega_{m1}$. However, no matter how the detuning Δ_p changes, there is still an invariant result, i.e., the dispersion shows a positive steep

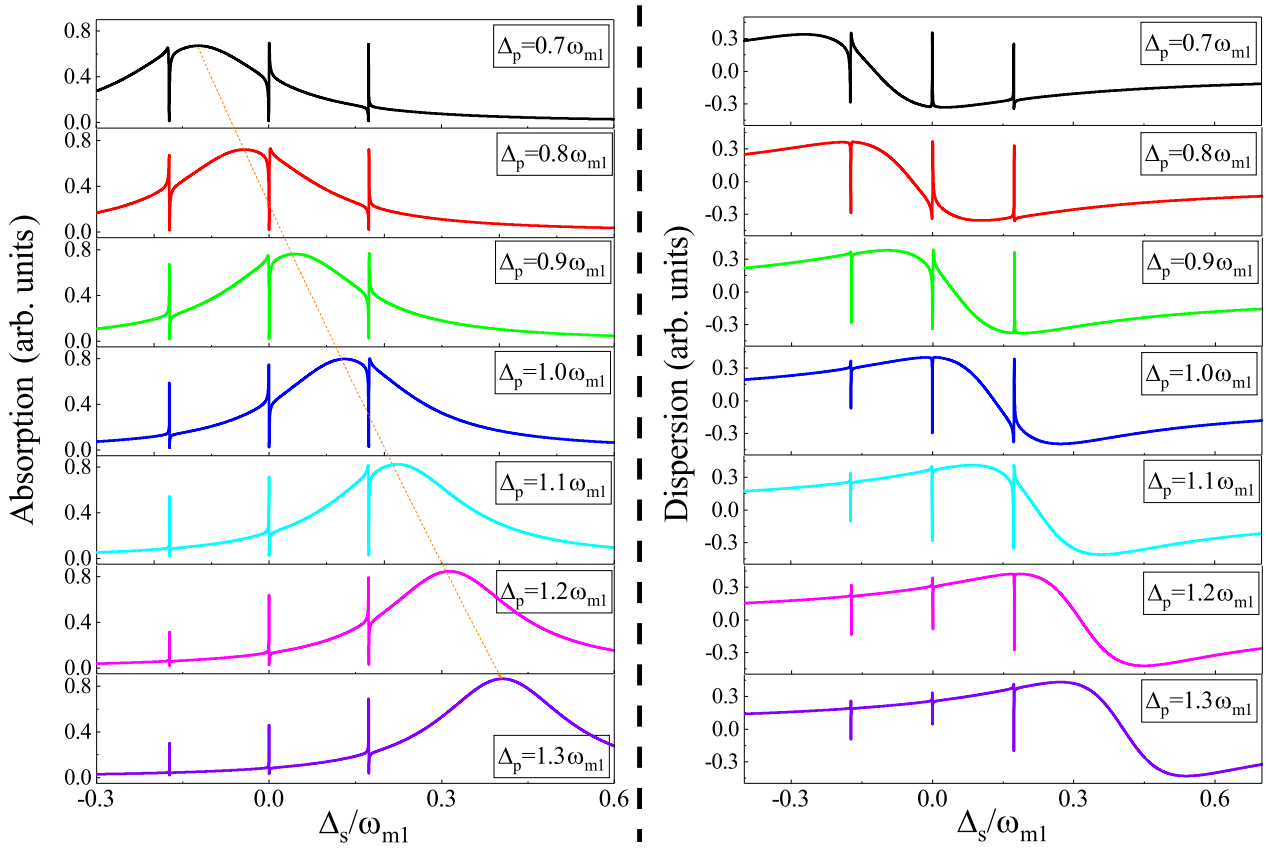

FIG. 5. Left: The probe absorption as a function of Δ_s for several different detuning Δ_p. Right: The dispersion as a function of Δ_s for several different detuning Δ_p. The other parameters are $\omega_{m1} = 1.2$ GHz, $\omega_{m2} = 0.9\omega_{m1}$, $\omega_{m3} = 1.1\omega_{m1}$, and $\Omega_p^2 = 0.1$ (GHz)^2.

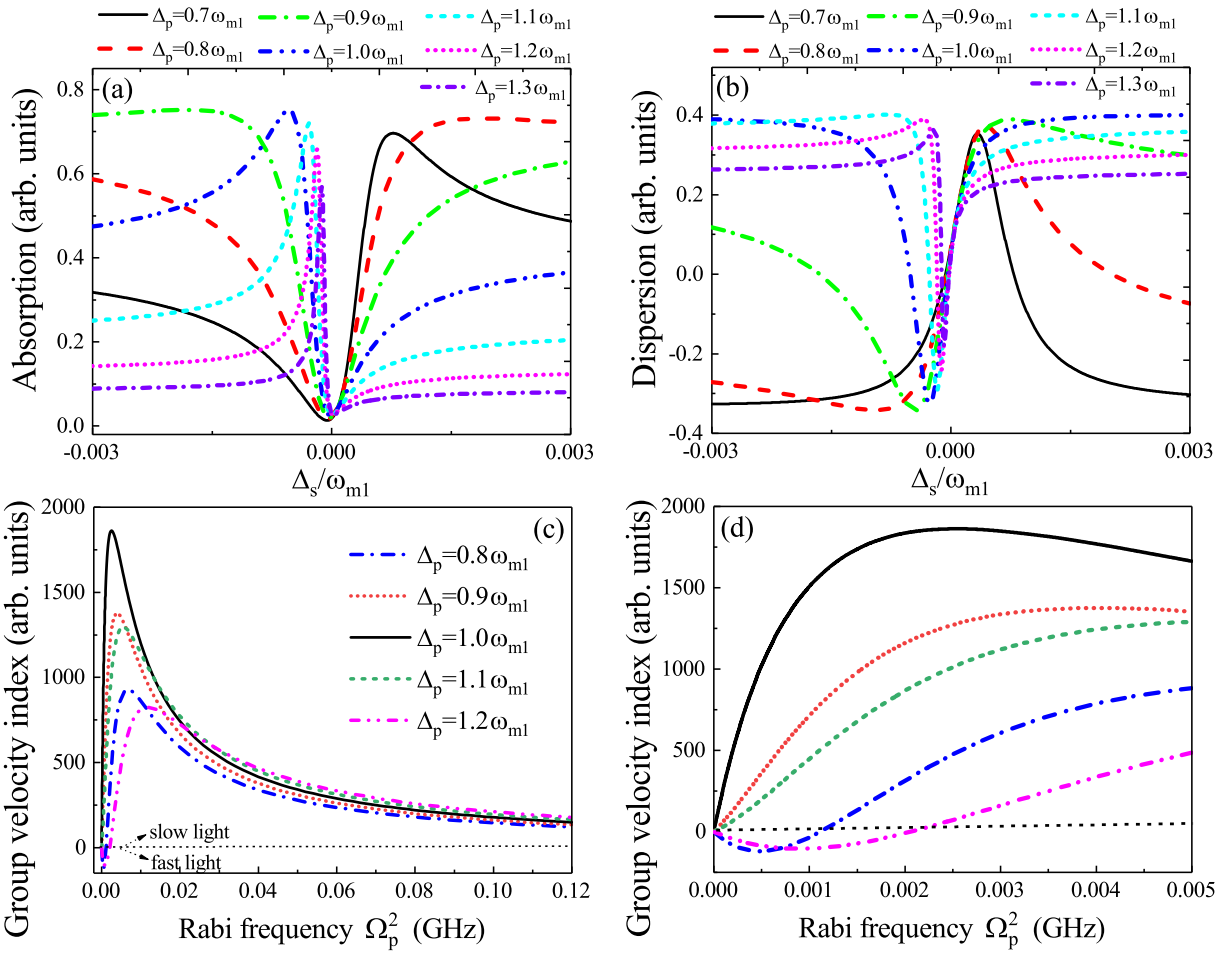

FIG. 6. (a) The details of the absorption of Fig. 5 around $\Delta_s = 0$. (b) The details of the dispersion of Fig. 5 around $\Delta_s = 0$. (c) The group velocity index n_g versus the Rabi frequency Ω_p^2 for several different Δ_p. (d) The detailed parts in (c). The other parameters are the same as in Fig. 5.

slope around $\Delta_s = 0$. Therefore, we also investigate the triple-Fano resonances that induce the coherent optical propagation properties as shown in Figs. 6(c) and 6(d). In Fig. 6(c), we plot the group velocity index n_g versus the Rabi frequency Ω_p^2 for different detuning Δ_p under the parameters as shown in Fig. 5. When the detuning Δ_p diverges from the red sideband $\Delta_p = \omega_{m1}$ (such as $\Delta_p = 0.8\omega_{m1}$ and $\Delta_p = 1.2\omega_{m1}$), the group velocity index n_g experiences the switch from fast light to slow light with increasing the Rabi frequency Ω_p^2 as shown by the double dot dashed pink line and dot dashed blue line in Fig. 6(c). However, if the detuning Δ_p approximates to $\Delta_p = \omega_{m1}$, only the slow light effect arrives in the system. The detailed parts are given in Fig. 6(d). Thus, with controlling the detuning regimes and the coupling strengths between the three NRs, the fast-to-slow light can be achieved straightforwardly in the hybrid system.

IV. CONCLUSION

In conclusion, we have proposed a hybrid NR system consisting of a suspended NR with an embedded QD driven by a pump field and a probe field is coupled to another two NRs with different frequencies via the Coulomb interaction, and we have investigated the absorption spectra of the probe field both under the conditions of the resonance ($\Delta_p = 0$) and off-resonance ($\Delta_p = \omega_{m1}$). In the situation of resonance, the sharp peaks in the absorption spectra depend on the interaction between the NRs. When in the off-resonance, we theoretically studied the multiple Fano resonance, and the positions and the shape of the multiple Fano line shapes are closely related to the detuning and the coupling strengths between the NRs. Moreover, the narrow transparency window in the probe transmission and the corresponding rapid phase dispersion allow for reaching the slow light effect. We have shown that the group velocity index of the probe field can be effectively tuned by the coupling strengths of the NRs and the pump detuning, and even obtain the conversion from slow light to fast light in the hybrid NR system.

As we elaborated that the NR **1** coupled to NR **2** and NR **3** via the Coulomb interaction, actually, the coupling between the NRs can be tuned by the gate voltage on the NRs, which has been demonstrated in coupled ion-nanomechanical systems [65,69]. When a gate voltage $V(t) = V_0 \cos(\omega_{ac} t)$ with frequency ω_{ac} is applied to the NRs via Ohmic contacts, the charge on the NRs oscillates with time and results in oscillating forces on the NRs [69]. Although we can reach the conversion from slow light to fast light based on the hybrid NR system, the total magnitude of slow light and fast light is determined by the number density of the QD and NRs.

Fortunately, an optically tunable delay of 50 ns and superluminal light with 1.4 ms signal advance have been observed with electromagnetically induced transparency in a cavity optomechanical system [67] which is very similar to our hybrid NR system. Then the results in the optomechanical system maybe give a reference to our NR system.

In addition, the hybrid coupled NRs system with coherent phonon manipulation will be not only useful for controlling classical oscillations but can also be extended to the quantum regime, which will open up the prospect of entangling two distinct macroscopic resonators [65]. Further, our proposal can also apply to photonics waveguide systems such as photonic nanocavities [70], especially the optomechanical crystals [71] in an optomechanical system [57], which is a particularly promising integration platform given the large attainable radiation-pressure coupling and the ability to create photonic and phononic band-gap waveguides. The advances in photonic integration have revealed the ability to interface hybrid material platforms to enhance light-matter interactions, which will lead to the development of on-chip signal processors and potential application in quantum information processing [72].

ACKNOWLEDGMENTS

H.-J.C. was supported by the National Natural Science Foundation of China (Grants No. 11647001 and No. 11804004). The project was funded by the China Postdoctoral Science Foundation (Grant No. 2020M681973) and the Anhui Provincial Natural Science Foundation (Grant No. 1708085QA11).

[1] M. O. Scully and M. S. Zubairy, Playing tricks with slow light, Science **301**, 181 (2003).
[2] R. W. Boyd and D. J. Gauthier, Controlling the velocity of light pulses, Science **326**, 1074 (2009).
[3] L. V. Hau, S. E. Harris, Z. Dutton, and C. H. Behroozi, Light speed reduction to 17 metres per second in an ultracold atomic gas, Nature (London) **397**, 594 (1999).
[4] D. Budker, D. F. Kimball, S. M. Rochester, and V. V. Yashchuk, Nonlinear Magneto-Optics and Reduced Group Velocity of Light in Atomic Vapor with Slow Ground State Relaxation, Phys. Rev. Lett. **83**, 1767 (1999).
[5] M. Fleischhauer, A. Imamoglu, and J. P. Marangos, Electromagnetically induced transparency: Optics in coherent media, Rev. Mod. Phys. **77**, 633 (2005).
[6] V. P. Kalosha, L. Chen, and X. Bao, Slow and fast light via SBS in optical fibers for short pulses and broadband pump, Opt. Express **14**, 12693 (2006).
[7] V. I. Kovalev, N. E. Kotova, and R. G. Harrison, Slow light in stimulated Brillouin scattering: on the influence of the spectral width of pump radiation on the group index: reply, Opt. Express **18**, 8055 (2010).
[8] M. S. Bigelow, N. N. Lepeshkin, and R. W. Boyd, Observation of Ultraslow Light Propagation in a Ruby Crystal at Room Temperature, Phys. Rev. Lett. **90**, 113903 (2003).
[9] S. Zhang, D. A. Genov, Y. Wang, M. Liu, and X. Zhang, Plasmon-Induced Transparency in Metamaterials, Phys. Rev. Lett. **101**, 047401 (2008).
[10] A. E. Miroshnichenko, S. Flach, and Y. S. Kivshar, Fano resonances in nanoscale structures, Rev. Mod. Phys. **82**, 2257 (2010).
[11] B. Luk'yanchuk, N. I. Zheludev, S. A. Maier, N. J. Halas, P. Nordlander, H. Giessen, and C. T. Chong, The Fano resonance in plasmonic nanostructures and metamaterials, Nat. Mater. **9**, 707 (2010).
[12] C. Wu, A. B. Khanikaev, and G. Shvets, Broadband Slow Light Metamaterial Based on a Double-Continuum Fano Resonance, Phys. Rev. Lett. **106**, 107403 (2011).
[13] U. Fano, Effects of configuration interaction on intensities and phase shifts, Phys. Rev. **124**, 1866 (1961).
[14] C. Liu, Z. Dutton, C. H. Behroozi, and L. V. Hau, Observation of coherent optical information storage in an atomic medium using halted light pulses, Nature (London) **409**, 490 (2001).
[15] S. E. Harris, J. E. Field, and A. Imamoglu, Nonlinear Optical Processes Using Electromagnetically Induced Transparency, Phys. Rev. Lett. **64**, 1107 (1990).
[16] J. Q. Shen and S. He, Nonlinear optical processes using electromagnetically induced transparency, Phys. Rev. A **74**, 063831 (2006).
[17] J. Q. Shen, Electromagnetically-induced-transparency plasmonics: Quantum-interference-assisted tunable surface-plasmon-polariton resonance and excitation, Phys. Rev. A **90**, 023814 (2014).
[18] S. Nojima, M. Usuki, M. Yawata, and M. Nakahata, Fano resonances for localized intrinsic defects in finite-sized photonic crystals, Phys. Rev. A **85**, 063818 (2012).
[19] J. Guo, L. Jiang, Y. Jia, X. Dai, Y. Xiang, and D. Fan, Low threshold optical bistability in one-dimensional gratings based on graphene plasmonics, Opt. Express **25**, 5972 (2017).
[20] A. Artar, Y. A. Ali, and H. Altug, Directional double Fano resonances in plasmonic hetero-oligomers, Nano Lett. **11**, 3694 (2011).
[21] S. Sasaki, H. Tamura, T. Akazaki, and T. Fujisawa, Fano-Kondo Interplay in a Side-Coupled Double Quantum Dot, Phys. Rev. Lett. **103**, 266806 (2009).
[22] Y. Yoon, M.-G. Kang, T. Morimoto, M. Kida, N. Aoki, J. L. Reno, Y. Ochiai, L. Mourokh, J. Fransson, and J. P. Bird, Coupling Quantum States through a Continuum: A Mesoscopic Multistate Fano Resonance, Phys. Rev. X **2**, 021003 (2012).
[23] B. Peng, S. K. Özdemir, W. Chen, F. Nori, and L. Yang, What is and what is not electromagnetically induced transparency in whispering-gallery microcavities, Nat. Commun. **5**, 5082 (2014).
[24] F. Lei, B. Peng, S. K. Özdemir, G. L. Long, and L. Yang, Dynamic Fano-like resonances in erbium-doped whispering-gallery-mode microresonators, Appl. Phys. Lett. **105**, 101112 (2014).
[25] Y. L. Li, J. Millen, and P. F. Barker, Simultaneous cooling of coupled mechanical oscillators using whispering gallery mode resonances, Opt. Express **24**, 1392 (2016).
[26] N. Verellen, Y. Sonnefraud, H. Sobhani, F. Hao, V. V. Moshchalkov, P. Van Dorpe, P. Nordlander, and S. A. Maier, Fano resonances in individual coherent plasmonic nanocavities, Nano Lett. **9**, 1663 (2009).

[27] J. Wallauer and M. Walther, Fano line shape and phase reversal in a split-ring resonator based metamaterial, Phys. Rev. B **88**, 195118 (2013).

[28] K.-L. Lee, S.-H. Wu, C.-W. Lee, and P.-K. Wei, Sensitive biosensors using Fano resonance in single gold nanoslit with periodic grooves, Opt. Express **19**, 24530 (2011).

[29] C. Wu, A. B. Khanikaev, R. Adato, N. Arju, A. A. Yanik, H. Altug, and G. Shvets, Fano-resonant asymmetric metamaterials for ultrasensitive spectroscopy and identification of molecular monolayers, Nat. Mater. **11**, 69 (2012).

[30] Z.-K. Zhou, X.-N. Peng, Z.-J. Yang, Z.-S. Zhang, M. Li, X.-R. Su, Q. Zhang, X. Shan, Q.-Q. Wang, and Z. Zhang, Tuning gold nanorod-nanoparticle hybrids into plasmonic Fano resonance for dramatically enhanced light emission and transmission, Nano Lett. **11**, 49 (2011).

[31] R. Taubert, M. Hentschel, J. Kästel, and H. Giessen, Classical analog of electromagnetically induced absorption in plasmonics, Nano Lett. **12**, 1367 (2012).

[32] M. Poot and H. S. J. van der Zant, Mechanical systems in the quantum regime, Phys. Rep. **511**, 273 (2013).

[33] B. Lassagne, Y. Tarakanov, J. Kinaret, D. Garcia-Sanchez, and A. Bachtold, Coupling mechanics to charge transport in carbon nanotube mechanical resonators, Science **325**, 1107 (2009).

[34] J. Tamayo, P. M. Kosaka, J. J. Ruz, A. S. Paulo, and M. Calleja, Biosensors based on nanomechanical systems, Chem. Soc. Rev. **42**, 1287 (2013).

[35] J. J. Li and K. D. Zhu, All-optical mass sensing with coupled mechanical resonator systems, Phys. Rep. **525**, 223 (2013).

[36] M. D. LaHaye, O. Buu, B. Camarota, and K. C. Schwab, Approaching the quantum limit of a nanomechanical resonator, Science **304**, 74 (2004).

[37] D. Rugar, R. Budakian, H. J. Mamin, and B. W. Chui, Single spin detection by magnetic resonance force microscopy, Nature (London) **430**, 329 (2004).

[38] M. D. LaHaye, J. Suh, P. M. Echternach, K. C. Schwab, and M. L. Roukes, Nanomechanical measurements of a superconducting qubit, Nature (London) **459**, 960 (2009).

[39] D. Hunger, S. Camerer, T. W. Hansch, D. Konig, J. P. Kotthaus, J. Reichel, and P. Treutlein, Resonant Coupling of a Bose-Einstein Condensate to a Micromechanical Oscillator, Phys. Rev. Lett. **104**, 143002 (2010).

[40] O. Arcizet, V. Jacques, A. Siria, P. Poncharal, P. Vincent, and S. Seidelin, A single nitrogen-vacancy defect coupled to a nanomechanical oscillator, Nat. Phys. **7**, 879 (2011).

[41] S. Kolkowitz, A. C. B. Jayich, Q. P. Unterreithmeier, S. D. Bennett, P. Rabl, J. G. E. Harris, and M. D. Lukin, Coherent sensing of a mechanical resonator with a single-spin qubit, Science **335**, 1603 (2012).

[42] J.-M. Pirkkalainen, S. U. Cho, Jian Li, G. S. Paraoanu, P. J. Hakonen, and M. A. Sillanpaa, Hybrid circuit cavity quantum electrodynamics with a micromechanical resonator, Nature (London) **494**, 211 (2013).

[43] A. D. O'Connell, M. Hofheinz, M. Ansmann, R. C. Bialczak, M. Lenander, E. Lucero, M. Neeley, D. Sank, H. Wang, M. Weides, J. Wenner, J. M. Martinis, and A. N. Cleland, Quantum ground state and single-phonon control of a mechanical resonator, Nature (London) **464**, 697 (2010).

[44] T. A. Palomaki, J. W. Harlow, J. D. Teufel, R. W. Simmonds, and K. W. Lehnert, Coherent state transfer between itinerant microwave fields and a mechanical oscillator, Nature (London) **495**, 210 (2013).

[45] I. Wilson-Rae, P. Zoller, and A. Imamoğlu, Laser Cooling of a Nanomechanical Resonator Mode to its Quantum Ground State, Phys. Rev. Lett. **92**, 075507 (2004),.

[46] S. D. Bennett, L. Cockins, Y. Miyahara, P. Grutter, and A. A. Clerk, Strong Electromechanical Coupling of an Atomic Force Microscope Cantilever to a Quantum Dot, Phys. Rev. Lett. **104**, 017203 (2010).

[47] I. Yeo, P. L. de Assis, A. Gloppe, E. Dupont-Ferrier, P. Verlot, N. S. Malik, E. Dupuy, J. Claudon, J. M. Gerard, A. Auffeves, G. Nogues, S. Seidelin, J. P. Poizat, O. Arcizet, and M. Richard, Strain-mediated coupling in a quantum dot-mechanical oscillator hybrid system, Nat. Nanotechnol. **9**, 106 (2014).

[48] K. C. Schwab and M. L. Roukes, Putting mechanics into quantum mechanics, Phys. Today **58**(7), 36 (2005).

[49] Y. J. Wang, M. Eardley, S. Knappe, J. Moreland, L. Hollberg, and J. Kitching, Magnetic Resonance in an Atomic Vapor Excited by a Mechanical Resonator, Phys. Rev. Lett. **97**, 227602 (2006).

[50] Y. T. Yang, C. Callegari, X. L. Feng, K. L. Ekinci, and M. L. Roukes, Zeptogram-scale nanomechanical mass sensing, Nano. Lett. **6**, 583 (2006).

[51] J. J. Li and K. D. Zhu, Tunable slow and fast light device based on a carbon nanotube resonator, Opt. Express **20**, 5840 (2012).

[52] P. C. Ma, J. Q. Zhang, Y. Xiao, M. Feng, and Z. M. Zhang, Tunable double optomechanically induced transparency in an optomechanical system, Phys. Rev. A **90**, 043825 (2014).

[53] Q. Yang, B. P. Hou, and D. G. Lai, Local modulation of double optomechanically induced transparency and amplification, Opt. Express **25**, 9697 (2017).

[54] Z. Qian, M. M. Zhao, B. P. Hou, and Y. H. Zhao, Tunable double optomechanically induced transparency in photonically and phononically coupled optomechanical systems, Opt. Express **25**, 33097 (2017).

[55] A. Zrenner, E. Beham, S. Stufler, F. Findeis, M. Bichler, and G. Abstreiter, Coherent properties of a two-level system based on a quantum-dot photodiode, Nature (London) **418**, 612 (2002).

[56] S. Stufler, P. Ester, A. Zrenner, and M. Bichler, Quantum optical properties of a single $In_xGa_{1-x}As$-GaAs quantum dot two-level system, Phys. Rev. B **72**, 121301(R) (2005).

[57] K. Fang, M. Matheny, X. Luan, and O. Painter, Optical transduction and routing of microwave phonons in cavity-optomechanical circuits, Nat. Photon. **10**, 489 (2016).

[58] Q. Wang, J. Q. Zhang, P. C. Ma, C. M. Yao, and M. Feng, Precision measurement of the environmental temperature by tunable double optomechanically induced transparency with a squeezed field, Phys. Rev. A **91**, 063827 (2015).

[59] W. K. Hensinger, D. W. Utami, H. S. Goan, K. Schwab, C. Monroe, and G. J. Milburn, Ion trap transducers for quantum electromechanical oscillators, Phys. Rev. A **72**, 041405(R) (2005).

[60] D. F. Walls and G. J. Milburn, in *Quantum Optics* (Springer-Verlag, Berlin, 1994), pp. 245–265.

[61] G. S. Agarwal and S. Huang, Electromagnetically induced transparency in mechanical effects of light, Phys. Rev. A **81**, 041803(R) (2010).

[62] R. W. Boyd, in *Nonlinear Optics* (Academic Press, San Diego, 1992), p. 225.

[63] S. E. Harris, J. E. Field, and A. Kasapi, Dispersive properties of electromagnetically induced transparency, Phys. Rev. A **46**, R29 (1992).

[64] R. S. Bennink, R. W. Boyd, C. R. Stroud, and V. Wong, Enhanced self-action effects by electromagnetically induced transparency in the two-level atom, Phys. Rev. A **63**, 033804 (2001).

[65] H. Okamoto, A. Gourgout, C. Y. Chang, K. Onomitsu, I. Mahboob, E. Y. Chang, and H. Yamaguchi, Coherent phonon manipulation in coupled mechanical resonators, Nat. Phys. **9**, 480 (2013).

[66] S. Weis, R. Riviere, S. Deleglise, E. Gavartin, O. Arcizet, A. Schliesser, and T. J. Kippenberg, Optomechanically induced transparency, Science **330**, 1520 (2010).

[67] A. H. Safavi-Naeini, T. P. M. Alegre, J. Chan, M. Eichenfield, M. Winger, Q. Lin, J. T. Hill, D. E. Chang, and O. Painter, Electromagnetically induced transparency and slow light with optomechanics, Nature (London) **472**, 69 (2011).

[68] J. D. Teufel, D. Li, M. S. Allman, K. Cicak, A. J. Sirois, J. D. Whittaker, and R. W. Simmonds, Circuit cavity electromechanics in the strong-coupling regime, Nature (London) **471**, 204 (2011).

[69] L. Tian and P. Zoller, Coupled Ion-Nanomechanical Systems, Phys. Rev. Lett. **93**, 266403 (2004).

[70] Y. Sato, Y. Tanaka, J. Upham, Y. Takahashi, T. Asano, and S. Noda, Strong coupling between distant photonic nanocavities and its dynamic control, Nat. Photon. **6**, 56 (2012).

[71] M. Eichenfield, J. Chan, R. M. Camacho1, K. J. Vahala, and O. Painter, Optomechanical crystals, Nature (London) **462**, 78 (2009).

[72] D. Marpaung, J. Yao, and J. Capmany, Integrated microwave photonics, Nat. Photon. **13**, 80 (2019).